

# Learning Gaussian-Bernoulli RBMs using Difference of Convex Functions Optimization

**Vidyadhar Upadhyा**

VIDYADHAR@EE.IISC.ERNET.IN

*Electrical Engineering Dept, Indian Institute of Science, Bangalore*

**P. S. Sastry**

SASTRY@EE.IISC.ERNET.IN

*Electrical Engineering. Dept, Indian Institute of Science, Bangalore*

## Abstract

The Gaussian-Bernoulli restricted Boltzmann machine (GB-RBM) is a useful generative model that captures meaningful features from the given  $n$ -dimensional continuous data. The difficulties associated with learning GB-RBM are reported extensively in earlier studies. They indicate that the training of the GB-RBM using the current standard algorithms, namely, contrastive divergence (CD) and persistent contrastive divergence (PCD), needs a carefully chosen small learning rate to avoid divergence which, in turn, results in slow learning. In this work, we alleviate such difficulties by showing that the negative log-likelihood for a GB-RBM can be expressed as a difference of convex functions if we keep the variance of the conditional distribution of visible units (given hidden unit states) and the biases of the visible units, constant. Using this, we propose a stochastic *difference of convex functions* (DC) programming (S-DCP) algorithm for learning the GB-RBM. We present extensive empirical studies on several benchmark datasets to validate the performance of this S-DCP algorithm. It is seen that S-DCP is better than the CD and PCD algorithms in terms of speed of learning and the quality of the generative model learnt.

**Keywords:** RBM, Gaussian-Bernoulli RBM, Contrastive Divergence, Difference of Convex Programming

## 1. Introduction

Probabilistic generative models are good for extracting meaningful representations from the data by learning high-dimensional multi-modal distributions in an unsupervised manner. The restricted Boltzmann machine (RBM) is one such generative model which was originally proposed for modeling distributions of binary data variables (called visible units) with the help of binary latent variables (called hidden units) (Smolensky, 1987; Freund and Haussler, 1992; Hinton, 2002). The RBM is found to be effective for unsupervised representation learning in several applications and has been used as a building block for models such as deep belief networks, deep Boltzmann machines (Hinton et al., 2006; Salakhutdinov and Hinton, 2009; Goh et al., 2014; Wang et al., 2019; Chen et al., 2018b) and also in combination with the Convolutional Neural Networks (Zhang et al., 2018). It can also be used as a discriminative model (Hinton et al., 2006; Zhang et al., 2019).

The RBM (like the Boltzmann machine) uses a suitable energy function to represent the probability distribution as a Gibbs distribution. The distinguishing feature of an RBM (compared to the Boltzmann machine) is that the hidden units are conditionally independent, conditioned on all the visible units and vice versa. These conditional distributions are

enough to define an energy function and hence, the joint distribution. The normalizing constant for the distribution, known as the partition function, is computationally intractable. However, one can efficiently sample from the distribution through Markov Chain Monte Carlo (MCMC) methods.

In the original RBM, both visible and hidden units are assumed to be binary. Hence, the model is also called Bernoulli-Bernoulli RBM (BB-RBM). It is to be noted that the visible units, being observable, constitute the data variables. To model continuous valued data, the binary visible units must be replaced with continuous ones though the hidden units can still remain binary. One possibility is to model the distribution of visible units conditioned on the hidden units as a Gaussian. The resulting model is called Gaussian-Bernoulli RBM (GB-RBM) (Welling et al., 2005; Hinton and Salakhutdinov, 2006). In this work, we address the important problem of finding efficient algorithms for learning GB-RBMs.

The usual approach to learning an RBM is by minimizing the KL divergence between the data and the model distributions which is equivalent to finding the maximum likelihood estimate of the parameters of the model. The maximum likelihood estimates have no closed form solution and the parameters are learnt using iterative algorithms to minimize the negative log likelihood. The log-likelihood gradient requires calculating an expectation *w.r.t.* the model distribution which is computationally expensive due to the presence of the intractable partition function. Therefore, this expectation is estimated using samples obtained from the model distribution using MCMC methods. This strategy is followed in the popular Contrastive Divergence (CD) algorithm and its variant, the Persistent Contrastive Divergence (PCD); the only algorithms currently used for learning GB-RBMs. However, the estimated gradient may have a large variance due to limitations in the MCMC procedure and can cause these stochastic gradient descent based algorithms to diverge sometimes (Cho et al., 2011). The issue of divergence is more prominent in the case of GB-RBM compared to BB-RBM (Wang et al., 2014).

It was shown in Lee et al. (2007) that learning GB-RBM with a sparse penalty provides meaningful representations for natural images. Although it was empirically observed that simple mixture models can outperform the GB-RBM models in terms of the likelihood estimation (Theis et al., 2011), with the re-parameterization of energy function and improved learning algorithm in Cho et al. (2011) the GB-RBM model was found to extract more meaningful representations. However, learning GB-RBM is a challenging task and difficulties associated with learning are reported extensively in the literature (Krizhevsky, 2009; Theis et al., 2011; Cho et al., 2011; Wang et al., 2014; Melchior et al., 2017). For instance, the analysis in Wang et al. (2014) showed that the failures in learning GB-RBMs are due to the inefficiency of training algorithms rather than any inherent limitations of the model itself. Several training recipes which make use of some knowledge of the data distribution were also suggested. They also showed that the features learnt on benchmark datasets are comparable to those learnt using sparse coding and Independent Component Analysis (ICA). This claim is theoretically justified in Karakida et al. (2016) where they showed that the GB-RBM, learnt using an exact maximum likelihood or an approximate maximum likelihood with CD estimates, extracts independent components at one of their stable fixed points. In addition, the difficulties to capture the geometric structure of the data manifold by GB-RBMs was overcome using approaches where the local manifold structure of the

data is captured through graph regularization (GraphRBM) (Chen et al., 2018a) and using the guidance from the available label information (pcGRBM) (Chu et al., 2019).

Currently, the CD and PCD algorithms are the standard algorithms for learning GB-RBM models. They require a carefully chosen learning rate (which is usually small) so as to avoid divergence of the log-likelihood. The small value of the learning rate results in slow convergence. In addition, one also needs careful parameter initialization and restriction of the gradient during the update, for avoiding the divergence of the log-likelihood. Thus, there is a need for an efficient algorithm for learning GB-RBMs.

In this work, we show that the log-likelihood function of a GB-RBM can be expressed as a difference of two convex functions under the assumption that the conditional distribution of visible units is Gaussian with unit variance. There are efficient algorithms for optimizing difference of convex functions and this strategy has been used earlier for learning BB-RBMs (Carlson et al., 2015; Nitanda and Suzuki, 2017; Upadhyay and Sastry, 2017). We adopt the stochastic difference of convex functions programming (S-DCP) (Upadhyay and Sastry, 2017) algorithm to learn GB-RBMs. Through extensive empirical studies using benchmark datasets, we show that the S-DCP algorithm is more efficient compared to the existing CD and PCD algorithms for learning GB-RBMs. The main contributions of this work are as follows.

We show that if the conditional distribution of the visible units is Gaussian with fixed variance, then the log likelihood function for GB-RBMs can be expressed as a difference of two convex functions. We then show how we can employ a two loop stochastic gradient descent algorithm (called S-DCP) to learn the GB-RBM and demonstrate through empirical studies that this algorithm is more efficient than CD and PCD. Though we fix the variance of the conditional distribution of the visible units in our algorithm, we still efficiently learn good representations. Further, we modify the S-DCP algorithm to accommodate variance update and show that the resulting method is also more efficient than CD and PCD. We show that the proposed algorithm is better in terms of the speed of learning, achieved log-likelihood, ability to extract meaningful features and to generate high quality samples.

The rest of the paper is organized as follows. In section 2, we briefly describe the RBM model and the maximum likelihood approach to learn a GB-RBM. We show that the GB-RBM log-likelihood is a difference of convex functions and describe the DC programming approach in section 3. In section 4, we describe the experimental setup and present the results. We conclude the paper in section 5.

## 2. Background

The RBM is a two layer recurrent neural network, in which  $m$  visible stochastic units (denoted as  $\mathbf{v}$ ) in one layer are connected to  $n$  hidden stochastic units (denoted as  $\mathbf{h}$ ) in the other (Rumelhart and McClelland, 1987; Freund and Haussler, 1992; Hinton, 2002). There are no connections among the units within each layer and the connections between the two layers are undirected. The weight of the connection between the  $i^{\text{th}}$  visible unit and the  $j^{\text{th}}$  hidden unit is denoted as  $w_{ij}$ . The bias for the  $i^{\text{th}}$  visible unit and the  $j^{\text{th}}$  hidden unit are denoted as  $b_i$  and  $c_j$ , respectively. Let  $\theta = \{\mathbf{w} \in \mathbb{R}^{n \times m}, \mathbf{b} \in \mathbb{R}^m, \mathbf{c} \in \mathbb{R}^n\}$  denote the parameters of the model. RBM represents probability distribution over the states of its

units as,

$$p(\mathbf{v}, \mathbf{h}|\theta) = e^{-E(\mathbf{v}, \mathbf{h}; \theta)} / Z(\theta), \quad (1)$$

where  $Z(\theta)$  is the normalizing constant, called the partition function and  $E(\mathbf{v}, \mathbf{h}; \theta)$  is the energy function. The bipartite connectivity structure in RBM implies conditional independence of visible units conditioned on all hidden units and vice-versa, i.e.,

$$p(\mathbf{v}|\mathbf{h}, \theta) = \prod_{i=1}^m p(v_i|\mathbf{h}, \theta), \quad p(\mathbf{h}|\mathbf{v}, \theta) = \prod_{i=1}^n p(h_i|\mathbf{v}, \theta).$$

## 2.1. Bernoulli-Bernoulli Restricted Boltzmann Machines

The RBM was originally proposed for binary visible and hidden units ( $\mathbf{v} \in \{0, 1\}^m$  and  $\mathbf{h} \in \{0, 1\}^n$ ). In the BB-RBM the conditional distributions are prescribed as,

$$\begin{aligned} p(v_i = 1|\mathbf{h}, \theta) &= \text{sigmoid} \left( b_i + \sum_{j=1}^n w_{ij} h_j \right) \\ p(h_j = 1|\mathbf{v}, \theta) &= \text{sigmoid} \left( c_j + \sum_{i=1}^m w_{ij} v_i \right) \end{aligned}$$

where,  $\text{sigmoid}(x) = 1/(1 + e^{-x})$  is the logistic sigmoid function. Using these, we obtain the following energy function.

$$E(\mathbf{v}, \mathbf{h}; \theta) = - \sum_{i,j} w_{ij} v_i h_j - \sum_{i=1}^m b_i v_i - \sum_{j=1}^n c_j h_j. \quad (2)$$

The data distribution represented by an RBM is that of the visible units which is obtained by marginalizing from eq. (1). One can show that any distribution over  $\{0, 1\}^m$  can be approximated by a BB-RBM with ( $m$  visible units and) sufficient number of hidden units (Montúfar and Rauh, 2017; Gu et al., 2019).

## 2.2. Gaussian-Bernoulli Restricted Boltzmann Machines

The BB-RBM can represent a data distribution only if the data variables are binary. The natural extension of the BB-RBM is to choose continuous visible units and binary hidden units, i.e.,  $\mathbf{v} \in \mathcal{R}^m$  and  $\mathbf{h} \in \{0, 1\}^n$ . In this case, the conditional distribution of the units are prescribed as,

$$\begin{aligned} p(v_i|\mathbf{h}, \theta) &= \mathcal{N} \left( v_i | b_i + \sum_j w_{ij} h_j, \sigma_i^2 \right) \\ p(h_j = 1|\mathbf{v}, \theta) &= \text{sigmoid} \left( c_j + \sum_i w_{ij} \frac{v_i}{\sigma_i^2} \right) \end{aligned} \quad (3)$$

where,  $\mathcal{N}(\cdot|\mu, \sigma^2)$  denotes Gaussian probability density function with mean  $\mu$  and variance  $\sigma^2$  Cho et al. (2011). This RBM model is called the Gaussian-Bernoulli RBM (GB-RBM).

The choice of the following energy function results in the desired conditional distributions as in eq. (3) ,

$$E(\mathbf{v}, \mathbf{h}|\theta) = \sum_i \frac{(v_i - b_i)^2}{2\sigma_i^2} - \sum_{i,j} \frac{w_{ij}v_i h_j}{\sigma_i^2} - \sum_j c_j h_j$$

where,  $\sigma_i^2$  is the variance associated with the  $i^{\text{th}}$  Gaussian visible unit (Cho et al., 2011). Using this energy function with  $\sigma_i^2 = 1, \forall i$ , we obtain (from eq. (1)) the partition function  $Z(\theta)$  as,

$$Z(\theta) = \sum_{\mathbf{h}} \int_{\mathbb{R}^m} e^{-\sum_i \frac{(v_i - b_i)^2}{2} + \sum_{i,j} w_{ij}v_i h_j + \sum_j c_j h_j} d\mathbf{v}.$$

### 2.3. Maximum Likelihood Learning

One can learn the GB-RBM parameters to represent the data distribution, given some training data, by maximizing the log-likelihood. For simplicity of notation, let us consider a single training sample ( $\mathbf{v}$ ). Then log-likelihood is given by,

$$\begin{aligned} \mathcal{L}(\theta|\mathbf{v}) &= \log p(\mathbf{v}|\theta) = \log \sum_{\mathbf{h}} p(\mathbf{v}, \mathbf{h}|\theta) \\ &\triangleq (g(\theta, \mathbf{v}) - f(\theta)) \end{aligned} \quad (4)$$

where,

$$\begin{aligned} g(\theta, \mathbf{v}) &= \log \sum_{\mathbf{h}} e^{-E(\mathbf{v}, \mathbf{h}; \theta)} \\ f(\theta) &= \log Z(\theta) = \log \sum_{\mathbf{h}} \int_{\mathbb{R}^m} e^{-E(\mathbf{v}, \mathbf{h}; \theta)} d\mathbf{v}. \end{aligned} \quad (5)$$

The required RBM parameters can be found as

$$\theta^* = \arg \max_{\theta} \mathcal{L}(\theta|\mathbf{v}) = \arg \max_{\theta} (g(\theta, \mathbf{v}) - f(\theta)).$$

Since there is no closed form solution, iterative gradient ascent procedure is used as,

$$\theta^{t+1} = \theta^t + \eta [\nabla_{\theta} g(\theta, \mathbf{v}) - \nabla_{\theta} f(\theta)]_{\theta=\theta^t}.$$

It is easily shown that the gradient of  $g$  and  $f$  are given by,

$$\begin{aligned} \nabla_{\theta} g(\theta, \mathbf{v}) &= -\mathbb{E}_{p(\mathbf{h}|\mathbf{v}; \theta)} [\nabla_{\theta} E(\mathbf{v}, \mathbf{h}; \theta)] \\ \nabla_{\theta} f(\theta) &= -\mathbb{E}_{p(\mathbf{v}, \mathbf{h}; \theta)} [\nabla_{\theta} E(\mathbf{v}, \mathbf{h}; \theta)]. \end{aligned} \quad (6)$$

Here,  $\mathbb{E}_q$  denotes the expectation *w.r.t.* the distribution  $q$ . Since  $\frac{\partial E(\mathbf{v}, \mathbf{h}; \theta)}{\partial w_{ij}} = -v_i h_j$ , we have,

$$\begin{aligned} \frac{\partial g(\theta, \mathbf{v})}{\partial w_{ij}} &= \sum_{\mathbf{h}} v_i h_j p(\mathbf{h}|\mathbf{v}, \theta) = v_i p(h_j = 1|\mathbf{v}, \theta) \\ &= v_i \sigma \left( c_j + \sum_{i=1}^m w_{ij} v_i \right). \end{aligned}$$

Similar to this case, the partial derivatives of  $g(\theta, \mathbf{v})$  w.r.t.  $b_i$  and  $c_j$  yield expressions that are analytically easy to evaluate.

In contrast, it is computationally very expensive to calculate  $\nabla_\theta f(\theta)$  due to the expectation in eq. (6). For example,

$$\begin{aligned}\frac{\partial f(\theta)}{\partial w_{ij}} &= \int_{\mathbb{R}^m} \sum_{\mathbf{h}} v_i h_j p(\mathbf{v}, \mathbf{h}|\theta) d\mathbf{v} \\ &= \int_{\mathbb{R}^m} v_i p(h_j = 1|\mathbf{v}, \theta) p(\mathbf{v}|\theta) d\mathbf{v}\end{aligned}$$

which is computationally hard. Hence, MCMC sampling methods are used to estimate the expectation to obtain  $\nabla_\theta f$ .

Due to the bipartite connectivity structure of the model, MCMC sampling can be efficiently implemented through block Gibbs sampler. This is followed in the contrastive divergence (CD) algorithm (Hinton, 2002) which is currently the most popular algorithm for learning GB-RBMs. In the CD( $k$ ) algorithm, the Markov chain is run for  $k$  block Gibbs sampling iterations and the  $k^{\text{th}}$  state is used for a single-sample approximation of the expectation. The training samples are used to initialize the Markov chain for every mini-batch. In a variant of this algorithm, called persistent contrastive divergence (PCD) (Tieleman, 2008), the Markov chain is initialized with the  $k^{\text{th}}$  state of the previous iteration's Markov chain.

Currently, CD and PCD are the standard algorithms used to train GB-RBMs. However, these algorithms are sensitive to hyperparameters and require a carefully chosen learning rate. Generally, the learning rate needs to be very small to avoid divergence and hence, these algorithms learn very slowly. This issue is more prominent in GB-RBMs for reasons described in Hinton (2010); Cho et al. (2011). As explained earlier, our objective is to train the GB-RBMs efficiently using algorithms that optimize the difference of convex functions.

### 3. Difference of Convex Functions Formulation

In this section, we show that the  $f$  and  $g$  functions given by eq. (5) are convex w.r.t.  $\mathbf{w}$  and  $\mathbf{c}$  under the assumption of fixed variance,  $\sigma_i^2$ . This implies that the log-likelihood function (considered as function of  $\mathbf{w}, \mathbf{c}$ ), given by eq. (4), is a difference of two convex functions. This property can be exploited to design efficient optimization algorithms through the *Difference of Convex* (DC) programming approach. Here we choose  $\sigma_i^2 = 1, \forall i$ , for the sake of convenience. It is easy to see that the result holds for any fixed value of  $\sigma_i^2$ .

#### 3.1. Convexity of $g(\theta, \mathbf{v})$

The function  $g(\theta, \mathbf{v})$  is given by,

$$g(\theta, \mathbf{v}) = \log \sum_{\mathbf{h}} e^{-\sum_i \frac{(v_i - b_i)^2}{2} + \sum_j c_j h_j + \sum_{i,j} w_{ij} v_i h_j}. \quad (7)$$

If the  $m \times n$  matrix,  $\mathbf{w}$ , is stacked to form a vector of dimension  $mn$ , denoted as  $vec(\mathbf{w})$ , then we can express eq. (7) as a function of  $\mathbf{w}$  and  $\mathbf{c}$  as,

$$g(\theta, \mathbf{v}) = \log \sum_{k=1}^{2^n} \beta_k e^{\mathbf{a}_k^T vec(\mathbf{w})} e^{\mathbf{h}^{(k)T} \mathbf{c}}$$

where,  $\beta_k = e^{-\sum_i \frac{(v_i - b_i)^2}{2}}$ ,  $\mathbf{a}_k = vec(\mathbf{v}(\mathbf{h}^{(k)})^T)$  and  $\mathbf{h}^{(k)}$ ,  $k = 1, \dots, 2^n$  are all the  $n$ -bit binary vectors or, equivalently, all possible values of the binary hidden vector  $\mathbf{h}$  (Note that  $\mathbf{v}(\mathbf{h}^{(k)})^T$  is a matrix of dimension  $m \times n$  and  $vec(\mathbf{v}(\mathbf{h}^{(k)})^T)$  is a vectorized version of it). The following Lemma now proves that  $g$  is convex w.r.t.  $\mathbf{w}$  and  $\mathbf{c}$ .

**Lemma 1** *A function of the following form is convex:*

$$lse_{\mathbf{a}}(\mathbf{u}) = \log \sum_{k=1}^N \beta_k e^{\mathbf{a}_k^T \mathbf{u}}$$

where,  $\mathbf{a}_1, \dots, \mathbf{a}_N$  are some fixed vectors in  $\mathbb{R}^d$  and  $\beta_k \geq 0, \forall k$ . (Note that the function  $lse_{\mathbf{a}}$  maps  $\mathbb{R}^d$  to  $\mathbb{R}$ ).

The proof of the above Lemma is given in appendix B.

Hence we can conclude that  $g$  is convex w.r.t.  $\mathbf{w}, \mathbf{c}$ . It is to be noted that the function  $g$  is not convex w.r.t.  $\mathbf{b}$ .

### 3.2. Convexity of $f(\theta)$

As shown in appendix A, we can write  $f(\theta)$  as,

$$f(\theta) = K_f + \log \sum_{\mathbf{h}} e^{\sum_j c_j h_j + \sum_i \left( \sum_j w_{ij} h_j \right) \left( \frac{\sum_j w_{ij} h_j}{2} + b_i \right)}.$$

This can also be expressed as,

$$f(\theta) = K_f + \log \sum_{k=1}^{2^n} \beta_k e^{s(k)} \quad (8)$$

where,  $s(k) = \frac{1}{2} \sum_i (\sum_j w_{ij} h_j^k)^2 + \sum_{i,j} w_{ij} h_j^k b_i$  and  $\beta_k = e^{\sum_j c_j h_j^k}$  with  $h_j^k$  being the  $j^{th}$  component of the binary vector  $\mathbf{h}^k$ . It is to be noted that  $\beta_k \geq 0, \forall k$ . Let the  $i^{th}$  row of  $\mathbf{w}$  be denoted as  $\mathbf{w}_{i*}$ . Then,

$$\left( \sum_j w_{ij} h_j^k \right)^2 = (\mathbf{w}_{i*}^T \mathbf{h}^k)^2 = \mathbf{w}_{i*}^T \mathbf{h}^k (\mathbf{h}^k)^T \mathbf{w}_{i*}.$$

Using the above and by treating  $vec(\mathbf{w})$  as an  $mn$ -dimensional vector where rows of  $\mathbf{w}$  are stacked one below the other (as done earlier), the eq. (8) can be rewritten in the following form,

$$f(\theta) = K_f + \log \sum_k e^{\mathbf{c}^T \mathbf{h}^{(k)}} e^{\frac{1}{2} vec(\mathbf{w})^T A_k vec(\mathbf{w}) + \mathbf{a}_k^T vec(\mathbf{w})} \quad (9)$$

Here,  $A_k$  is an  $mn \times mn$  block diagonal matrix in which each block is a rank one matrix of the form  $\mathbf{h}^k(\mathbf{h}^k)^T$  and  $\mathbf{a}_k = \text{vec}(\mathbf{b}(\mathbf{h}^k)^T)$  is a vector of dimension  $mn$ . The form of  $A_k$  ensures that it is a positive semi-definite matrix. The following Lemma now proves  $f$  is convex *w.r.t.*  $\mathbf{w}, \mathbf{c}$ .

**Lemma 2** *A function of the form*

$$\text{lse}_q(\mathbf{u}) = \log \sum_i \beta_i e^{\frac{1}{2} \mathbf{u}^T A_i \mathbf{u} + \mathbf{a}_i^T \mathbf{u}}$$

*is convex if the matrix  $A_i$  is positive semi-definite and  $\beta_i \geq 0, \forall i$ .*

The proof of the above Lemma is given in appendix C.<sup>1</sup>

Having proved that both  $f$  and  $g$  are convex *w.r.t.*  $\mathbf{w}$  and  $\mathbf{c}$ , we can now conclude, using eq. (4), that the log-likelihood function of the GB-RBM is a difference of convex functions *w.r.t.* weights,  $\mathbf{w}$ , and bias of hidden units,  $\mathbf{c}$ .

### 3.3. Difference of Convex Functions Optimization

The difference of convex programming (DCP) (Yuille et al., 2002; An and Tao, 2005) is a method used for solving optimization problems of the form,

$$\theta^* = \arg \min_{\theta} F(\theta) = \arg \min_{\theta} (f(\theta) - g(\theta)),$$

where, both  $f$  and  $g$  are convex functions of  $\theta$ . In the RBM setting,  $F$  corresponds to the negative log-likelihood and the functions  $f$  and  $g$  correspond to those defined in eq. (5). While both  $f$  and  $g$  are convex and smooth,  $F$  is non-convex.

The DCP is an iterative procedure defined by,

$$\theta^{(t+1)} = \arg \min_{\theta} \left( f(\theta) - \theta^T \nabla g(\theta^{(t)}) \right). \quad (10)$$

Note that the optimization problem on the RHS of eq. (10) is convex and hence, the DCP consists of solving a convex optimization problem in each iteration. It can be shown, using convexity of  $f$  and  $g$ , that the iterates defined by eq. (10) constitute a descent method for minimizing  $F$  (Yuille et al., 2002; An and Tao, 2005). One can also show that the iterates would constitute a descent on  $F$  as long as a descent on the objective function in (the RHS of) eq. (10) is ensured at each iteration even if this optimization problem is not solved exactly. Such an approach, called the stochastic-DC programming (S-DCP) algorithm, was proposed earlier for learning BB-RBMs (Upadhyay and Sastry, 2017).

In the S-DCP algorithm, the convex optimization problem described in eq.(10) is solved (approximately) using a fixed  $d$  number of iterations of stochastic gradient descent (*w.r.t.*  $\theta$ ) on  $f(\theta) - \theta^T \nabla g(\theta^{(t)}, \mathbf{v})$ . For this, the  $\nabla f$  is estimated using samples obtained through MCMC, as in the case of CD (the estimate is denoted as  $\hat{f}'(\theta, \mathbf{v})$ ). The S-DCP algorithm is described in detail via Algorithm 1.

---

1. We call the function in Lemma 2 as a log-sum-exponential-quadratic function and hence, the notation  $\text{lse}_q$ . While the convexity of  $\text{lse}$  functions given by (12) in appendix B is known, we do not know of any discussion or reported proofs of convexity of the  $\text{lse}_q$  functions considered here.

---

**Algorithm 1** S-DCP update for a single training sample  $\mathbf{v}$  (Upadhyay and Sastry, 2017). The estimate of the  $\nabla f$  is denoted as  $\hat{f}'(\theta, \mathbf{v})$ .

---

**Input:**  $\mathbf{v}, \theta^{(t)} = \{\mathbf{w}^{(t)}, \mathbf{c}^{(t)}\}, \eta, d, K'$   
 Initialize  $\tilde{\theta}^{(0)} = \theta^{(t)}, \tilde{\mathbf{v}}^{(0)} = \mathbf{v}$   
**for**  $l = 0$  **to**  $d - 1$  **do**  
   **for**  $k = 0$  **to**  $K' - 1$  **do**  
     sample  $h_i^{(k)} \sim p(h_i | \tilde{\mathbf{v}}^{(k)}, \tilde{\theta}^{(l)})$ ,  $\forall i$   
     sample  $\tilde{v}_j^{(k+1)} \sim p(v_j | \mathbf{h}^{(k)}, \tilde{\theta}^{(l)})$ ,  $\forall j$   
   **end for**  
    $\tilde{\theta}^{(l+1)} = \tilde{\theta}^{(l)} - \eta \left[ \hat{f}'(\tilde{\theta}^{(l)}, \tilde{\mathbf{v}}^{(K')}) - \nabla g(\theta^{(t)}, \mathbf{v}) \right]$   
    $\tilde{\mathbf{v}}^{(0)} = \tilde{\mathbf{v}}^{(K')}$   
**end for**  
**Output:**  $\theta^{(t+1)} = \tilde{\theta}^{(d)}$

---

If the computational cost of one Gibbs transition is  $T$  and that of evaluating gradient of  $g$  (or  $f$ ) is  $L$ , the computational cost of the CD- $K$  algorithm for a mini-batch of size  $N_B$  is  $N_B(KT + 2L)$  whereas the S-DCP algorithm has cost  $dN_B(K'T + L) + N_BL$  when  $K'$  MCMC steps and  $d$  inner loop iterations are chosen (Upadhyay and Sastry, 2017). It may be noted that, by choosing the S-DCP hyperparameters  $d$  and  $K'$  such that  $KT = dK'T + (d - 1)L$ , the amount of computations required is approximately same as that for CD algorithm with  $K$  steps (Upadhyay and Sastry, 2017). If we assume that  $(d - 1)L$  is small, then the computational cost of both CD and S-DCP algorithms can be made approximately equal by choosing  $dK' = K$ . However, S-DCP updates the parameter  $(\theta)$   $d$  times per mini-batch whereas CD updates the parameter only once per mini-batch. Therefore, S-DCP computational cost is slightly more compared to CD (refer table 2 for the comparison of the exact computational time for different algorithms).

In sections 3.1 and 3.2 we showed that the functions  $f$  and  $g$  are convex only with respect to the parameters  $\mathbf{w}$  and  $\mathbf{c}$ . Hence, the S-DCP cannot be directly used for learning the biases of the visible units,  $\mathbf{b}$ . We could update  $\mathbf{b}$  outside the S-DCP loop using the same update as in CD. Instead, we fix this parameter to be the mean of the data directly without training, as suggested in Melchior et al. (2017). Our experimental results show that even with a fixed  $\mathbf{b}$ , we could still learn good models.

With regard to the variance parameter, the choice of  $\sigma_i^2 = 1, \forall i$ , indicates that we learn a Gaussian with unit variance as the conditional distribution of visible units. Therefore, we suitably normalize the input data to ensure unit variance and compare the performance of the S-DCP algorithm with that of the CD and PCD algorithms. We also explore the performance of these algorithms when the variance parameter not fixed, but is learnt by the model. In this case, only  $\mathbf{w}$  and  $\mathbf{c}$  are updated in the inner loop of the S-DCP algorithm and the variance parameter is updated only once per mini-batch outside the S-DCP loop. We use the re-parameterization of the variance parameter as in Cho et al. (2011) to constrain them to stay positive during the update. A detailed description of this variant of the S-DCP algorithm is given in Algorithm 2.

---

**Algorithm 2** S-DCP update for a single training sample  $\mathbf{v}$  when learning variance

---

**Input:**  $\mathbf{v}, \theta^{(t)} = \{\mathbf{w}^{(t)}, \mathbf{c}^{(t)}\}, \boldsymbol{\sigma}^{(t)}, \eta, d, K'$   
 Initialize  $\tilde{\theta}^{(0)} = \theta^{(t)}, \tilde{\mathbf{v}}^{(0)} = \mathbf{v}$   
**for**  $l = 0$  **to**  $d - 1$  **do**  
   **for**  $k = 0$  **to**  $K' - 1$  **do**  
     sample  $h_i^{(k)} \sim p(h_i | \tilde{\mathbf{v}}^{(k)}, \tilde{\theta}^{(l)})$ ,  $\forall i$   
     sample  $\tilde{v}_j^{(k+1)} \sim p(v_j | \mathbf{h}^{(k)}, \tilde{\theta}^{(l)})$ ,  $\forall j$   
   **end for**  
    $\tilde{\theta}^{(l+1)} = \tilde{\theta}^{(l)} - \eta \left[ \hat{f}'(\tilde{\theta}^{(l)}, \tilde{\mathbf{v}}^{(K')}) - \nabla g(\theta^{(t)}, \mathbf{v}) \right]$   
    $\tilde{\mathbf{v}}^{(0)} = \tilde{\mathbf{v}}^{(K')}$   
**end for**  
 Update  $\boldsymbol{\sigma}$  using re-parameterization as in [Cho et al. \(2011\)](#).  
**Output:**  $\theta^{(t+1)} = \tilde{\theta}^{(d)}, \boldsymbol{\sigma}^{(t+1)}$

---

## 4. Experiments and Discussion

### 4.1. Datasets

In order to analyse the performance of the different algorithms, we consider four benchmark grey scale image datasets namely Natural images ([van Hateren J H and van der Schaaf A, 1998](#)), Olivetti faces ([Samaria and Harter, 1994](#)), MNIST ([LeCun et al., 2012](#)) and Fashion-MNIST (FMNIST) ([Xiao et al., 2017](#)). The details of each of these datasets, the data dimension ( $m$ ), number of training samples ( $N_{tr}$ ) and number of test samples ( $N_{te}$ ) along with the other hyperparameters of algorithms (to be explained in Section 4.2) are provided in Table 1.

Table 1: The Details of the Datasets and the Hyperparameters

Dataset	$m$	$N_{tr}$	$N_{te}$	$n$	$N_E$	$N_B$	$K$	$d$	$K'$
Nat. Images	196	$40K$	$30K$	196	200	100	12	3	4
MNIST	784	$60K$	$10K$	200	300	200	24	4	6
FMNIST	784	$60K$	$10K$	200	300	200	24	4	6
Olivetti Faces	4096	400	—	500	3000	10	12	3	4

Similar to [Wang et al. \(2014\)](#) the Natural images dataset used is a subset of the Van Hateren's Natural image database ([van Hateren J H and van der Schaaf A, 1998](#)). These images are whitened using Zero-phase Component Analysis (ZCA). As mentioned in section 2, the features learnt using GB-RBM on this dataset are comparable to those learnt using sparse coding and Independent Component Analysis (ICA) ([Wang et al., 2014](#)).

In addition to the Natural image dataset, we also consider the Olivetti faces dataset which was used to study deep Boltzmann machines ([Cho et al., 2013](#)). There are ten different images for each of the 40 subjects in this dataset. They are whitened using ZCA. All the images are used to train the GB-RBM model primarily because the number of data samples are less in this dataset. Training using all the images also alleviates the sensitivity

issues of the RBM (RBMs are sensitive to translation in images) which could be caused by the mismatch in the alignment of training and testing images.

The MNIST dataset contains handwritten digits, whereas the FMNIST contains images of fashion products. All these images are normalized to have mean 0 and variance 1.

#### 4.2. Experimental setup

For each dataset, the hyperparameters such as the number of hidden nodes ( $n$ ), mini-batch size ( $N_B$ ) etc are chosen to be the same across all the algorithms, as provided in Table 1. The learning rate ( $\eta$ ) is chosen separately for each algorithm as the maximum possible value (such that, increasing it further will cause divergence of the log-likelihood). The number of hidden nodes (denoted by  $n$ ) in the RBM models for different datasets is shown in Table 1. To study the speed of learning, we train the GB-RBM model for a fixed number of epochs (denoted as  $N_E$  in Table 1). In each epoch, the mini-batch learning procedure is employed and the training data is shuffled after every epoch. In order to get an unbiased comparison, we did not use momentum or weight decay in any of the algorithms.

We evaluate the algorithms using the performance measures obtained from multiple trials, where each trial fixes the initial configuration of the weights and biases as follows. The weights are initialized to samples drawn from a uniform distribution with support  $[-a, a]$  where,  $a = 6/\sqrt{m+n}$ . The bias of the hidden units is initialized to  $c_j = -\frac{\|b-W_{*j}\|^2 - \|b\|^2}{2} + \log \tau_j$ , as proposed in [Wang et al. \(2014\)](#) where,  $\tau_j$  is fixed to 0.01. The bias of the visible units ( $\mathbf{b}$ ) is not learnt (as explained in the section 3.3) but fixed to the mean of the training samples.

We compare the performance of S-DCP with CD and PCD keeping the computational complexity of S-DCP roughly the same as that of CD/PCD by choosing  $K, d$  and  $K'$  such that  $K = dK'$  ([Upadhyay and Sastry, 2017](#)). We have experimentally observed that a large  $K$  generally results in a sensible generative model, also supported by the findings from [Wang et al. \(2014\)](#); [Carlson et al. \(2015\)](#). Therefore, we choose  $K = 24$  in CD and PCD (with  $d = 4, K' = 6$  for S-DCP) for learning MNIST and FMNIST datasets and we choose  $K = 12$  in CD and PCD (with  $d = 3, K' = 4$  for S-DCP) for the other two datasets, as shown in Table 1.

The algorithms are implemented using Python and CUDAMat (a CUDA-based matrix class for Python bindings) ([Mnih, 2009](#)) on a system with Intel processor *i7* – 7700 (4 CPU cores and processor base frequency 3.60 GHz), NVIDIA Titan X Pascal GPU and a 16 GB RAM configuration.

#### 4.3. Evaluation Criterion

We compare the performance of different algorithms based on the following criteria: speed of learning, quality and generalization capacity of the learnt model, quality of the learnt filters and generative ability of the learnt model.

We use the achieved log-likelihood on the train and the test samples to evaluate the quality of learnt models ([Hinton, 2010](#)). While the achieved average train log-likelihood provides a reasonable measure to compare the quality of the learnt model, its evolution (over epochs) indicates the speed of learning. The average train log-likelihood (denoted as

ATLL) is evaluated as,

$$ATLL = \frac{1}{N} \sum_{i=1}^N \log p(\mathbf{v}_{train}^{(i)} | \theta) \quad (11)$$

where,  $\mathbf{v}_{train}^{(i)}$  denotes the  $i^{\text{th}}$  training sample. The average test log-likelihood (denoted as ATeLL), on the other hand, provides a good indication of the generalization capacity of the model. Similar to ATLL, we evaluate the average test log-likelihood by using the test samples rather than the training samples. The computation of ATLL and ATeLL require the estimate of the partition function. It is estimated using annealed importance sampling (Neal, 2001) with 100 particles and 10000 intermediate distributions according to a linear temperature scale between 0 and 1. In the following section, we show the evolution (over epochs) of mean and maximum (over all trials) of the average train and test log-likelihood, for all the algorithms considered, for both the cases of fixed variance and learnt variance.

The learning procedure is effective when the weights learnt by the model are able to capture the important/crucial features of the dataset. Therefore, we interpret the model weights as filters and examine the filters learnt. The evaluation in terms of the generative ability of the learnt models is carried out by observing the samples that these models generate. For this, we randomly initialize the states of the visible units (in the learnt model) and run the alternating Gibbs Sampler for 200 steps and plot the state of the visible units.

#### 4.4. Performance Comparison

##### 4.4.1. SPEED OF LEARNING

As mentioned in section 4.2 all the three algorithms have comparable computational load (per mini-batch) if we select  $K = dK'$ . However, the computations performed by the different algorithms are not identical (S-DCP updates the parameter  $d$  times per mini-batch whereas CD updates the parameter only once per mini-batch). Therefore, we present the actual computational time of different algorithms. Table 2 provides the mean and the standard deviation ( $\sigma_t$ ) of the utilized time (in seconds), computed over 20 trials, for a fixed 100 epochs of learning by each of the algorithms for the different datasets considered. As seen from the table, the computation time per epoch is roughly the same for all algorithms.

Table 2: The system time statistics (The mean and standard deviation of the system time in seconds) for different datasets

Algorithm	Natural Images		Olivetti Faces		MNIST/FMNIST	
	Mean	$\sigma_t$	Mean	$\sigma_t$	Mean	$\sigma_t$
CD	40.42	0.29	7.96	0.03	77.94	0.19
PCD	41.74	0.26	8.03	0.03	79.05	0.15
S-DCP	43.87	0.23	9.19	0.02	88.64	0.11

To compare the speed of learning as well as the quality of the learnt models, we plot the progress of the *normalized* mean average train log-likelihood over epochs for different

Table 3: The number of epochs and system time statistics (in seconds) for achieving the reference normalized mean average log-likelihood by different algorithms for each datasets.

Dataset	Ref. LL (%)	CD		PCD		S-DCP	
		Epoch	Time	Epoch	Time	Epoch	Time
Nat. Images	95	125	50.52	125	52.17	60	<b>29.39</b>
MNIST	95	247	192.51	160	126.48	100	<b>88.64</b>
FMNIST	95	183	142.63	120	94.86	79	<b>70.02</b>
Olivetti Faces	80	2400	191.04	1750	140.52	1500	<b>137.85</b>

algorithms in Fig. 1. The log-likelihood is normalized using min-max normalization to restrict the range between 0 and 1, and to easily compare the learning speeds. For each dataset we take the maximum and minimum log-likelihoods among all algorithms to do this normalization. From Fig. 1, we observe that the log-likelihood achieved at the end of training is different for each algorithm. The average train log-likelihood achieved by the S-DCP algorithm is superior to those achieved by the CD and PCD algorithms across all datasets.

In order to better illustrate the efficiency of the S-DCP algorithm, we choose a reference log-likelihood (denoted as Ref. LL), as shown in Fig. 1. For the Natural image, MNIST and FMNIST datasets the Ref. LL is chosen as 95% (i.e., 95% of the highest ATLL achieved). For the Olivetti faces dataset we choose the Ref. LL as the maximum log-likelihood achieved by the CD algorithm (since CD attains the least log-likelihood among all the algorithms) which is approximately 80% of the maximum. Table 3 provides the Ref. LL along with the number of epochs and the computational time required to achieve this for the different algorithms.

Both, Table 3 and Fig. 1, demonstrate that the S-DCP algorithm is much faster compared to other algorithms both in terms of the number of epochs and the actual computational time. For instance, the speed of learning on the Natural image dataset, indicated in the Fig. 1 by the epoch at which the model achieves 95% of the highest mean ATLL, shows that CD and PCD algorithms require around 60 more epochs of training compared to the S-DCP algorithm which translates to approximately twice the required computation time. On MNIST and FMNIST datasets, S-DCP is approximately twice as fast as CD and 1.4 times as fast as the PCD. On Olivetti faces dataset, the CD algorithm achieves only 80% of the final log-likelihood achieved by the S-DCP algorithm and S-DCP achieves this value approximately 900 and 250 epochs earlier than CD and PCD, respectively. In terms of the computational time (to learn the Olivetti faces dataset) S-DCP takes about 25% less time compared to CD though the times taken by PCD and S-DCP are about the same.

Thus, we find that S-DCP has a higher speed of learning compared to the other algorithms. We also observed a similar behaviour when the normalized maximum ATLL is considered instead of normalized mean ATLL.

#### 4.4.2. QUALITY AND GENERALIZATION CAPACITY

As mentioned earlier, the quality of the trained model could be captured by the average train log-likelihood (ATLL) and the generalization capacity could be inferred from the average

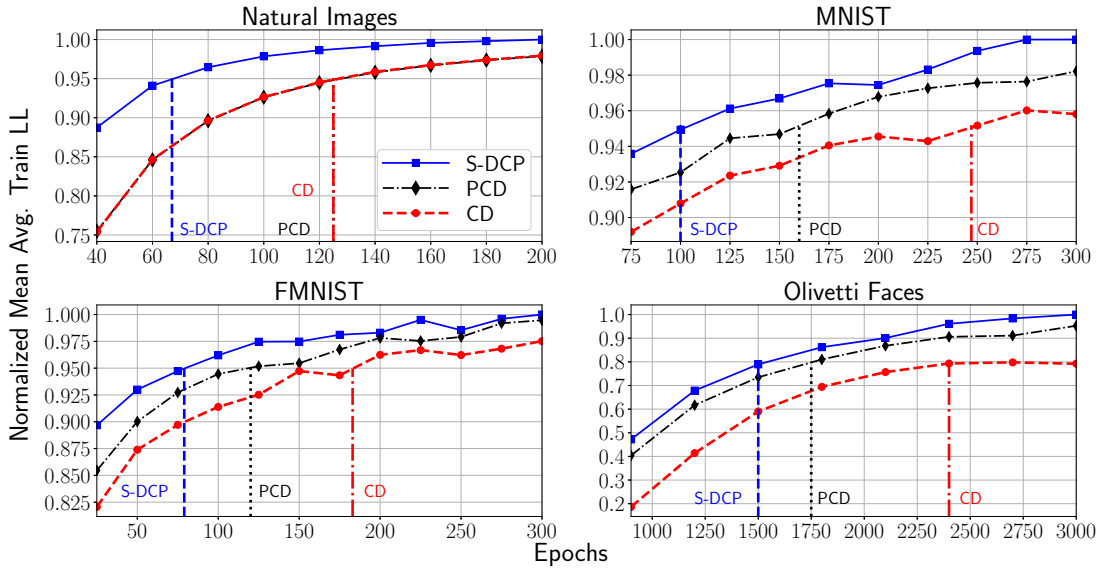


Figure 1: The normalized mean average train log-likelihood achieved with different algorithms on all the datasets with fixed variance. For S-DCP, Algorithm 1 is used.

test log-likelihood (ATeLL). We now show these results in both the cases of fixed variance and learnt variance.

**Fixed Variance:** The evolution of the train and the test log-likelihoods shown in Fig. 2, for each dataset, demonstrates that the S-DCP algorithm performs consistently better compared to the other two algorithms across all the datasets.

**Learning Variance:** The evolution of the train and the test log-likelihoods, over epochs, when the variance parameter is also learnt using the Algorithm 2, is shown in Fig. 3 for different datasets. We observe that in this case also S-DCP outperforms both the CD and PCD algorithms.

The higher train and test log-likelihood (across datasets) achieved by the S-DCP compared to those achieved using CD and PCD indicates the better quality and generalization capacity of the models learnt using the S-DCP algorithm.

In Fig. 4, we plot the typical evolution of the variance as learning progresses for Natural images and MNIST dataset using CD and S-DCP algorithm (We have observed that PCD learns similar models as that of CD in terms of learnt variance and hence to avoid clutter PCD plots are omitted). We selected two visible units, and plot the mean (over 20 trials) of the variances of these two units as learning evolves. We also show the variance over 20 trials of this evolution as a shaded region around the plot of the mean. These two units seem to be typical of a large number of visible units. All units start with unit variance and most units either settle to a variance close to 1 or much lower.

From the Fig. 4, we observe that both CD and S-DCP converge to approximately similar variance values though S-DCP converges faster. We have observed similar behaviour with the other two datasets.

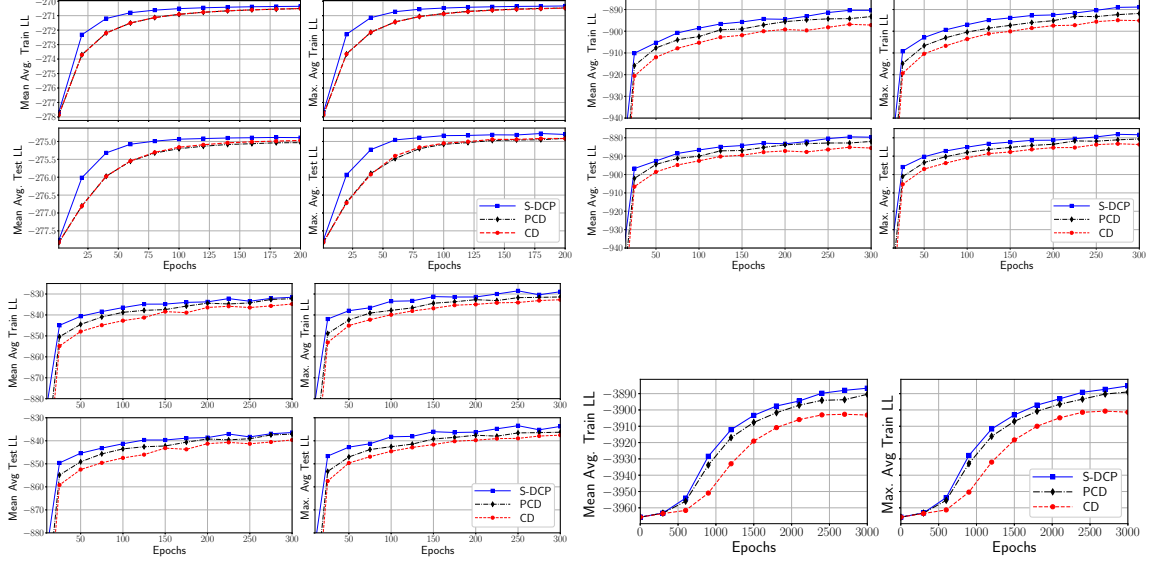


Figure 2: The performance of different algorithms on each dataset with fixed variance. For S-DCP, Algorithm 1 is used. (Note that, unlike in Fig. 1, here we show the evolution of log likelihood starting from the first epoch; consequently here the range of  $y$ -axis is more and hence the scale on  $y$ -axis is compressed).

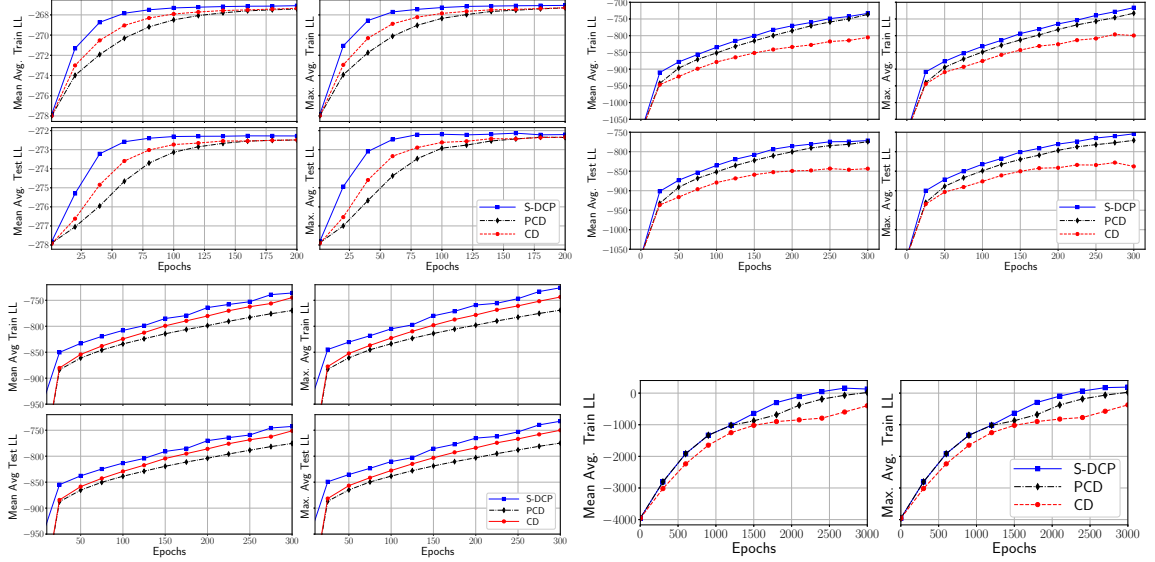


Figure 3: The performance of different algorithms on each dataset while also learning variance. For S-DCP, Algorithm 2 is used. It may be noted that the average train log-likelihood for the Olivetti faces dataset evolves to reach positive value since the learnt variance is small and contributes high negative value to the log partition function.

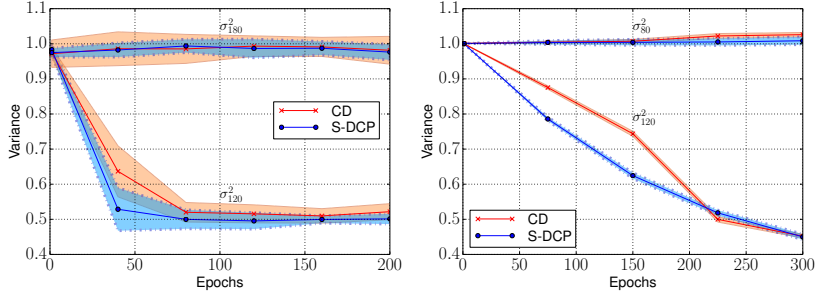


Figure 4: The evolution of the variance of two specific visible units as learning progresses by CD and S-DCP algorithms on Natural images and MNIST dataset. For S-DCP, Algorithm 2 is used.

#### 4.4.3. QUALITY OF THE LEARNT FILTERS

We next look at the filters learnt by different algorithms. In the following discussion, we present the results only for the fixed variance case. The same conclusions hold true even in the case of learning the variance.

A few sample weights from the model learnt (at the end of epochs at which the Ref. LL is achieved) are plotted as filters in Fig. 5. To do so, the set of weights connected to each hidden unit (of dimension  $m$ ) is reshaped to the original image size and plotted as grey scale images.

As observed from the Fig. 4.4.3 and 4.4.3, the weights are able to capture the relevant information from the training data. Specifically, we observe that the filters capture the edge related information in the Natural Images dataset (4.4.3) and extract the facial features from the Olivetti faces dataset (4.4.3). Thus, we find that S-DCP learns filters comparable to those learnt by CD and PCD; but it learns them faster.

Models tend to learn point filters in the initial stages of training and slowly converge to edge-like filters when mean zero and unit variance normalization is used instead of ZCA. This phenomenon was observed in Krizhevsky (2009) on natural images. The same phenomenon is observed here in Fig. 4.4.3 and Fig. 4.4.3, for the MNIST and FMNIST datasets. From the figures we find that most of the filters have only been able to capture the point-like information from the data. However, we observe that S-DCP results in more filters that capture edge-like information compared to the CD and PCD algorithms. This indicates that the transition from point filters to edge filters happens earlier with the S-DCP algorithm.

#### 4.4.4. GENERATIVE ABILITY

The samples from the models learnt (at the end of epochs at which the Ref. LL is achieved) using different algorithms are given in Fig. 6. From the figure we observe that the model learnt using S-DCP generates samples that are sharper and less noisy compared to those generated by the models learnt using the CD and PCD algorithms.

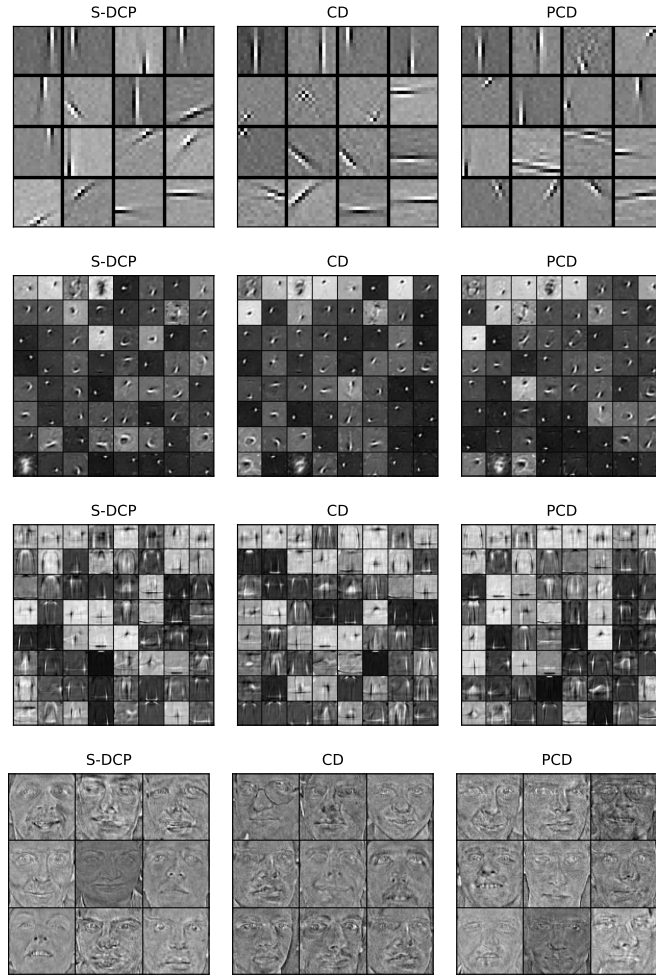


Figure 5: A few sample weights (obtained at the end of epochs at which the Ref. LL is achieved) or filters learnt using different algorithms on each dataset with fixed variance (For S-DCP, Algorithm 1 is used) are plotted as grey-scale images.

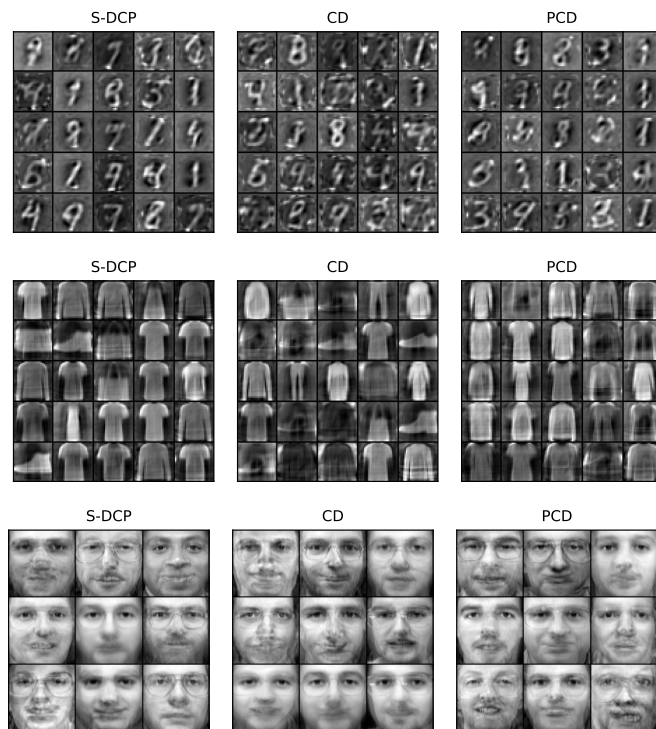


Figure 6: The samples from the models learnt (at the end of epochs at which the Ref. LL is achieved) using different algorithms on each dataset with fixed variance. For S-DCP, Algorithm 1 is used.

## 5. Conclusions

While GB-RBMs are good models for unsupervised representation learning, training them successfully is a challenging task. The current standard algorithms namely, CD and PCD are very sensitive to the hyperparameters and hence, are not very efficient to train GB-RBMs. In this work, we showed that the negative log-likelihood of a GB-RBM is a difference of convex functions with respect to the weights,  $w_{ij}$ , and the biases of hidden units,  $c_j$  (under the assumption that the variances of visible units are fixed) and this is utilized to employ the difference of convex functions programming approach to propose an efficient algorithm, called S-DCP. We also proposed a variant of S-DCP where the learning of this variance is also facilitated. Through extensive empirical results on multiple datasets, we showed that S-DCP results in a considerable improvement in the speed of learning and the quality of the final generative models learnt compared to those of CD and PCD. The results presented in this study support the claim that the S-DCP algorithm is currently a very efficient method to learn GB-RBMs. In the S-DCP algorithm, the noisy gradient estimated through MCMC sampling is used for optimizing a convex function and this may be the reason why the optimization method is more effective compared to CD and PCD. Further work is needed in terms of theoretical analysis of such stochastic gradient descent on convex functions to better understand the optimization dynamics of S-DCP and to possibly further improve it. Another direction in which the work presented here can be extended is in terms of exploring the utility of second order methods based on estimated Hessian in the inner loop of the S-DCP which solves a convex optimization problem.

## Appendix A. The function $f$

Consider the partition function,

$$\begin{aligned}
Z(\theta) &= \sum_{\mathbf{h}} \int_{\mathbf{v}} e^{-\sum_i \frac{(v_i - b_i)^2}{2} + \sum_{i,j} w_{ij} v_i h_j + \sum_j c_j h_j} d\mathbf{v} \\
&= \sum_{\mathbf{h}} e^{\sum_j c_j h_j + \sum_i (\sum_j w_{ij} h_j) \left( \frac{\sum_j w_{ij} h_j}{2} + b_i \right)} \times \\
&\quad \int_{\mathbf{v}} e^{-\sum_i \frac{(v_i - (\sum_j w_{ij} h_j + b_i))^2}{2}} d\mathbf{v} \\
&= (2\pi)^{\frac{m}{2}} \sum_{\mathbf{h}} e^{\sum_j c_j h_j + \sum_i (\sum_j w_{ij} h_j) \left( \frac{\sum_j w_{ij} h_j}{2} + b_i \right)}.
\end{aligned}$$

Therefore,  $f(\theta) = \log Z(\theta)$  is given by,

$$f(\theta) = K_f + \log \sum_{\mathbf{h}} e^{\sum_j c_j h_j + \sum_i (\sum_j w_{ij} h_j) \left( \frac{\sum_j w_{ij} h_j}{2} + b_i \right)}$$

where,  $K_f = \frac{m}{2} \log(2\pi)$ .

## Appendix B. Convexity of log-sum-exponential function

We first prove that  $lse$  function ( $\mathbb{R}^d \rightarrow \mathbb{R}$ ) given by,

$$lse(\mathbf{u}) = \log \sum_i \beta_i e^{u_i} = \log \beta^T e^{\mathbf{u}} \quad (12)$$

is convex *w.r.t.*  $\mathbf{u}$ . Here,  $u_i$  denotes  $i^{\text{th}}$  element of the vector  $\mathbf{u}$  and  $e^{\mathbf{u}}$  denotes element-wise exponential of  $\mathbf{u}$ . The gradient and Hessian of  $lse$  are given as,

$$\begin{aligned} \nabla lse(\mathbf{u}) &= \frac{\beta \odot e^{\mathbf{u}}}{\beta^T e^{\mathbf{u}}} \\ \nabla^2 lse(\mathbf{u}) &= \frac{\beta^T e^{\mathbf{u}} \text{diag}(\beta \odot e^{\mathbf{u}}) - (\beta \odot e^{\mathbf{u}})(\beta \odot e^{\mathbf{u}})^T}{(\beta^T e^{\mathbf{u}})^2} \\ &= \frac{\text{diag}(\beta \odot e^{\mathbf{u}})}{\beta^T e^{\mathbf{u}}} - \left( \frac{\beta \odot e^{\mathbf{u}}}{\beta^T e^{\mathbf{u}}} \right) \left( \frac{\beta \odot e^{\mathbf{u}}}{\beta^T e^{\mathbf{u}}} \right)^T \end{aligned}$$

where,  $\odot$  denotes element-wise multiplication. Let us denote,  $\mathbf{a} = \beta \odot e^{\mathbf{u}}$ . Now, the Hessian can be written as,

$$\nabla^2 lse(\mathbf{u}) = \frac{\text{diag}(\mathbf{a})}{\mathbf{1}^T \mathbf{a}} - \frac{\mathbf{a} \mathbf{a}^T}{(\mathbf{1}^T \mathbf{a})^2}$$

where,  $\mathbf{1}$  is a vector of all 1's. Now we have,

$$\begin{aligned} \mathbf{x}^T \nabla^2 lse(\mathbf{u}) \mathbf{x} &= \mathbf{x}^T \left( \frac{\mathbf{1}^T \mathbf{a} \text{diag}(\mathbf{a}) - \mathbf{a} \mathbf{a}^T}{(\mathbf{1}^T \mathbf{a})^2} \right) \mathbf{x} \\ &= \frac{\sum a_k \sum a_k x_k^2 - (\sum a_k x_k)^2}{(\sum a_k)^2} \geq 0. \end{aligned}$$

Hence, the  $lse$  function given in eq. (12) is convex. Now, consider the function of the form (given in Lemma 1),

$$lse_{\mathbf{a}}(\mathbf{u}) = \log \sum_{i=1}^N \beta_i e^{\mathbf{a}_i^T \mathbf{u}} \quad (13)$$

where,  $\mathbf{a}_1, \dots, \mathbf{a}_N$  are some fixed vectors in  $\mathbb{R}^d$ . Let  $A$  be an  $N \times d$  matrix whose rows are  $\mathbf{a}_i$ , then  $lse_{\mathbf{a}}(\mathbf{s}) = lse(A\mathbf{s})$ . Now, for any two vectors  $\mathbf{s}_1, \mathbf{s}_2 \in \mathbb{R}^d$  we have,

$$\begin{aligned} lse_{\mathbf{a}}(\alpha \mathbf{s}_1 + (1 - \alpha) \mathbf{s}_2) &= lse(A(\alpha \mathbf{s}_1 + (1 - \alpha) \mathbf{s}_2)) \\ &\leq \alpha lse(A\mathbf{s}_1) + (1 - \alpha) lse(A\mathbf{s}_2) \\ &= \alpha lse_{\mathbf{a}}(\mathbf{s}_1) + (1 - \alpha) lse_{\mathbf{a}}(\mathbf{s}_2). \end{aligned}$$

Hence, the  $lse_{\mathbf{a}}$  function is convex which proves Lemma 1.

## Appendix C. Convexity of log-sum-exponential-quadratic function

Consider the log-sum-exponential-quadratic function,

$$lse_q(\mathbf{u}) = \log \sum_i \beta_i e^{\frac{1}{2} \mathbf{u}^T A_i \mathbf{u} + \mathbf{a}_i^T \mathbf{u}}.$$

The gradient of the above function is,

$$\nabla lse_q(\mathbf{u}) = \frac{\sum_i \beta_i e^{\frac{1}{2}\mathbf{u}^T A_i \mathbf{u} + \mathbf{a}_i^T \mathbf{u}} (A_i \mathbf{u} + \mathbf{a}_i)}{\sum_i \beta_i e^{\frac{1}{2}\mathbf{u}^T A_i \mathbf{u} + \mathbf{a}_i^T \mathbf{u}}}.$$

Let  $\gamma(i) = \beta_i e^{\frac{1}{2}\mathbf{u}^T A_i \mathbf{u} + \mathbf{a}_i^T \mathbf{u}}$  and  $\bar{\gamma}(i) = \frac{\gamma(i)}{\sum_i \gamma(i)}$ . The Hessian of  $lse_q(\mathbf{u})$  is given as,

$$\begin{aligned} \nabla^2 lse_q(\mathbf{u}) &= \sum_i \bar{\gamma}(i) A_i + \sum_i \bar{\gamma}(i) (A_i \mathbf{u} + \mathbf{a}_i) (A_i \mathbf{u} + \mathbf{a}_i)^T \\ &\quad - \sum_i \bar{\gamma}(i) (A_i \mathbf{u} + \mathbf{a}_i) \sum_i \bar{\gamma}(i) (A_i \mathbf{u} + \mathbf{a}_i)^T. \end{aligned}$$

Now, consider  $\mathbf{x}^T \nabla^2 lse_q(\mathbf{u}) \mathbf{x}$ ,

$$\mathbf{x}^T \nabla^2 lse_q(\mathbf{u}) \mathbf{x} = \sum_i \bar{\gamma}(i) \mathbf{x}^T A_i \mathbf{x} + \sum_i \bar{\gamma}(i) \alpha_i^2 - \left( \sum_i \bar{\gamma}(i) \alpha_i \right)^2$$

where,  $\alpha_i = \mathbf{x}^T (A_i \mathbf{u} + \mathbf{a}_i)$ . By noting that  $\sum_i \bar{\gamma}(i) \alpha_i^2 - (\sum_i \bar{\gamma}(i) \alpha_i)^2 \geq 0$ , we can write

$$\mathbf{x}^T \nabla^2 lse_q(\mathbf{u}) \mathbf{x} \geq \sum_i \bar{\gamma}(i) \mathbf{x}^T A_i \mathbf{x}.$$

If  $A_i, \forall i$  is positive semi-definite then  $\mathbf{x}^T \nabla^2 lse_q(\mathbf{u}) \mathbf{x} \geq 0$ . Therefore, the log-sum-exponential-quadratic functions of the considered form are convex.

## Acknowledgment

The authors thank the NVIDIA Corporation for the donation of the Titan X Pascal GPU used in this research.

## References

Le Thi Hoai An and Pham Dinh Tao. The DC (difference of convex functions) programming and DCA revisited with DC models of real world nonconvex optimization problems. *Annals of Operations Research*, 133(1):23–46, 2005. ISSN 1572-9338. .

David Carlson, Volkan Cevher, and Lawrence Carin. Stochastic spectral descent for restricted Boltzmann machines. In *Proceedings of the Eighteenth International Conference on Artificial Intelligence and Statistics*, pages 111–119, 2015.

D. Chen, J. Lv, and Z. Yi. Graph regularized restricted Boltzmann machine. *IEEE Transactions on Neural Networks and Learning Systems*, 29(6):2651–2659, June 2018a. ISSN 2162-2388. .

X. Chen, J. Weng, W. Lu, J. Xu, and J. Weng. Deep manifold learning combined with convolutional neural networks for action recognition. *IEEE Transactions on Neural Networks and Learning Systems*, 29(9):3938–3952, 2018b.

K. H. Cho, T. Raiko, and A. Ilin. Gaussian-Bernoulli deep Boltzmann machine. In *The 2013 International Joint Conference on Neural Networks (IJCNN)*, pages 1–7, Aug 2013.

KyungHyun Cho, Alexander Ilin, and Tapani Raiko. Improved Learning of Gaussian-Bernoulli Restricted Boltzmann Machines. In *Artificial Neural Networks and Machine Learning – ICANN 2011*, pages 10–17. Springer Berlin Heidelberg, 2011. ISBN 978-3-642-21735-7.

J. Chu, H. Wang, H. Meng, P. Jin, and T. Li. Restricted Boltzmann machines with Gaussian visible units guided by pairwise constraints. *IEEE Transactions on Cybernetics*, 49(12):4321–4334, Dec 2019.

Yoav Freund and David Haussler. Unsupervised learning of distributions on binary vectors using two layer networks. In *Advances in Neural Information Processing Systems 4*, pages 912–919. Morgan-Kaufmann, 1992.

H. Goh, N. Thome, M. Cord, and J. Lim. Learning deep hierarchical visual feature coding. *IEEE Transactions on Neural Networks and Learning Systems*, 25(12):2212–2225, 2014.

L. Gu, J. Huang, and L. Yang. On the representational power of restricted Boltzmann machines for symmetric functions and boolean functions. *IEEE Transactions on Neural Networks and Learning Systems*, 30(5):1335–1347, May 2019. ISSN 2162-2388.

G. E. Hinton and R. R. Salakhutdinov. Reducing the dimensionality of data with neural networks. *Science*, 313(5786):504–507, 2006. ISSN 0036-8075. .

Geoffrey Hinton. A practical guide to training restricted Boltzmann machines. *Momentum*, 9(1):926, 2010.

Geoffrey E Hinton. Training products of experts by minimizing contrastive divergence. *Neural computation*, 14(8):1771–1800, 2002.

Geoffrey E. Hinton, Simon Osindero, and Yee Whye Teh. A fast learning algorithm for deep belief nets. *Neural Computation*, 18:1527–1554, 2006.

Ryo Karakida, Masato Okada, and Shun ichi Amari. Dynamical analysis of contrastive divergence learning: Restricted Boltzmann machines with Gaussian visible units. *Neural Networks*, 79:78 – 87, 2016. ISSN 0893-6080. .

Alex Krizhevsky. Learning Multiple Layers of Features from Tiny Images. Master’s thesis, Computer Science Department, University of Toronto, 2009.

Yann A. LeCun, Léon Bottou, Genevieve B. Orr, and Klaus-Robert Müller. Efficient Back-Prop. *Neural Networks: Tricks of the Trade: Second Edition*, pages 9–48, 2012.

Honglak Lee, Chaitanya Ekanadham, and Andrew Y. Ng. Sparse deep belief net model for visual area V2. In *Proceedings of the 20th International Conference on Neural Information Processing Systems*, pages 873–880, Red Hook, NY, USA, 2007. ISBN 9781605603520.

Jan Melchior, Wang Nan, and Wiskott Laurenz. Gaussian-binary restricted Boltzmann machines for modeling natural image statistics. *PLOS ONE*, 12(2):1–24, Feb 2017. .

Volodymyr Mnih. Cudamat: a CUDA-based matrix class for Python. 2009.

Guido Montúfar and Johannes Rauh. Hierarchical models as marginals of hierarchical models. *International Journal of Approximate Reasoning*, 88:531–546, 2017. ISSN 0888-613X. .

Radford M Neal. Annealed importance sampling. *Statistics and Computing*, 11(2):125–139, 2001.

Atsushi Nitanda and Taiji Suzuki. Stochastic Difference of Convex Algorithm and its Application to Training Deep Boltzmann Machines. In *Proceedings of the 20th International Conference on Artificial Intelligence and Statistics*, volume 54 of *Proceedings of Machine Learning Research*, pages 470–478, 20–22 Apr 2017.

D. E. Rumelhart and J. L. McClelland. Information processing in dynamical systems: Foundations of harmony theory. *Parallel Distributed Processing: Explorations in the Microstructure of Cognition: Foundations*, pages 194–281, 1987.

Ruslan Salakhutdinov and Geoffrey E Hinton. Deep Boltzmann machines. In *AISTATS*, volume 1, page 3, 2009.

F. S. Samaria and A. C. Harter. Parameterisation of a stochastic model for human face identification. In *Proceedings of 1994 IEEE Workshop on Applications of Computer Vision*, pages 138–142, Dec 1994. .

P. Smolensky. Information processing in dynamical systems: Foundations of harmony theory. In D. E. Rumelhart and J. L. McClelland, editors, *Parallel Distributed Processing: Explorations in the Microstructure of Cognition: Foundations*, pages 194–281, 1987.

Lucas Theis, Sebastian Gerwinn, Fabian Sinz, and Matthias Bethge. In all likelihood, deep belief is not enough. *Journal of Machine Learning Research*, 12(94):3071–3096, 2011.

Tijmen Tieleman. Training restricted Boltzmann machines using approximations to the likelihood gradient. In *Proceedings of the 25th International Conference on Machine Learning*, pages 1064–1071. Association for Computing Machinery, 2008. ISBN 9781605582054.

Vidyadhar Upadhyay and P. S. Sastry. Learning RBM with a DC programming approach. In *Proceedings of the Ninth Asian Conference on Machine Learning*, volume 77 of *Proceedings of Machine Learning Research*, pages 498–513. PMLR, 15–17 Nov 2017.

van Hateren J H and van der Schaaf A. Independent component filters of natural images compared with simple cells in primary visual cortex. *Proceedings of the Royal Society B: Biological Sciences*, 265(1394):359–366, Mar 1998. ISSN 0962-8452 1471-2954.

G. Wang, J. Qiao, J. Bi, Q. Jia, and M. Zhou. An adaptive deep belief network with sparse restricted Boltzmann machines. *IEEE Transactions on Neural Networks and Learning Systems*, pages 1–12, 2019.

Nan Wang, Jan Melchior, and Laurenz Wiskott. Gaussian-binary restricted boltzmann machines on modeling natural image statistics. *CoRR*, abs/1401.5900, 2014.

Max Welling, Michal Rosen-zvi, and Geoffrey E Hinton. Exponential Family Harmoniums with an Application to Information Retrieval. In *Advances in Neural Information Processing Systems 17*, pages 1481–1488. MIT Press, 2005.

Han Xiao, Kashif Rasul, and Roland Vollgraf. Fashion-MNIST: A novel image dataset for benchmarking machine learning algorithms, 2017.

Alan L Yuille, Anand Rangarajan, and AL Yuille. The concave-convex procedure (CCCP). *Advances in neural information processing systems*, 2:1033–1040, 2002.

Ji Zhang, Hongjun Wang, Jielei Chu, Shudong Huang, Tianrui Li, and Qigang Zhao. Improved Gaussian-Bernoulli restricted Boltzmann machine for learning discriminative representations. *Knowledge-Based Systems*, 185:104911, 2019. ISSN 0950-7051.

Jian Zhang, Shifei Ding, and Nan Zhang. An overview on probability undirected graphs and their applications in image processing. *Neurocomputing*, 321:156 – 168, 2018. ISSN 0925-2312.